RSC Advances

PAPER

View Article Online
View Journal | View Issue

Cite this: *RSC Adv.*, 2017, **7**, 42505

Adsorption and separation properties of positively charged ZrO_2 nanofibrous membranes fabricated by electrospinning

Yufei Tang, Zhaowei Liu, Kang Zhao * and Song Fu

Received 26th July 2017
Accepted 29th August 2017

DOI: 10.1039/c7ra08227d

rsc.li/rsc-advances

As a new type of adsorption and separation materials, positively charged ceramics exhibit the advantages of safety and high separation efficiency. However, these materials possess low specific surface area and adsorption capacity. In this study, positively charged ZrO_2 nanofibrous membranes were fabricated by electrospinning and calcination. The membranes were characterized in terms of morphology, composition, and pore structure. The adsorption and separation performance of the membranes on titan yellow solution was also investigated. Overlapping electrospun nanofibers formed nanofibrous membranes with porous structures (pore size of 0.2–1.6 μm) and a high specific surface area. Increasing the nanofiber diameter decreased the specific surface area of the nanofibrous membranes, and vacuum calcination increased their surface positive charge. The maximum flux of the positively charged ZrO_2 nanofibrous membranes reached 523 L $(m^2\ h)^{-1}$, and the interception rate for titan yellow was 99.997%. The saturated adsorption capacity of vacuum-calcined ZrO_2 nanofibrous membranes increased with increasing specific surface area, and their maximum adsorption capacity reached 20.93 mg cm^{-3}.

Introduction

In materials science, viruses and bacteria are charged colloidal particles.[1] Most viruses or bacteria in nature are negatively charged.[2,3] In 1991, scholars proposed the separation of viruses by using positively charged porous materials with fixed charges on the surface.[4] This method utilizes not only the physical separation of pores but also the electrostatic adsorption of positive charges on the surface, and the resultant large-pore materials can absorb small-sized bacteria and viruses. Porous ceramics incorporated in positively charged materials exhibit high-temperature resistance, chemical resistance, microbial resistance, and high mechanical properties[5,6] and can be recycled by high temperature and ultraviolet radiation after the separation of bacteria and viruses.[7,8] Nanoporous Al_2O_3 coatings prepared on the surface of activated carbon particles can increase the isoelectric point of the surface and the removal efficiency of *Escherichia coli* MS2.[9] In a previous study, positively charged ZrO_2 or Y_2O_3 nanocoating was loaded on diatomite by impregnation and sintering;[10,11] the coating showed a removal rate of 99% for *E. coli* MS2 but exhibited a low specific surface area (8 $m^2\ g^{-1}$), which led to low adsorption capacity for other bacteria and viruses. Hence, micro/nanoporous ceramic membranes with high porosity, specific surface area, and adsorption capacity[12,13] should be used as adsorbent materials to effectively separate and remove negatively charged viruses and bacteria.

Porous ceramic membranes with high porosity and specific surface area can be easily prepared by electrospinning.[14,15] Oxide nanofibrous membranes prepared by electrospinning possess a high specific surface area of 10–100 $m^2\ g^{-1}$.[16–18] In addition, ceramic nanofibers exhibit a small diameter and can be spliced into porous membranes, with pore sizes of 0.05–2.0 μm;[19] these nanofibers are used for physical separation because of their high adsorption capacity for viruses and bacteria. In this study, positively charged ZrO_2 nanofibrous membranes were fabricated by electrospinning. ZrO_2 was chosen on the basis of potential data for the material, which indicated that it could exhibit a positive surface charge across a wide pH range and will achieve high interception rate and adsorption capacity. The membranes obtained by vacuum calcination exhibited higher isoelectric point than those fabricated in air. The membranes were also characterized in terms of morphology and physical properties, and their adsorption and separation performance for titan yellow (mimovirus surface charge) was investigated under different environmental conditions. The fabricated positively charged ZrO_2 nanofibrous membranes exhibit potential for infectious virus protection, water treatment, pharmaceutical production, and biological engineering.

Department of Materials Science and Engineering, Xi'an University of Technology, Xi'an 710048, PR China. E-mail: kzhao@xaut.edu.cn; Fax: +86 29 82312922; Tel: +86 29 82312922

Experimental

Materials and methods

Zirconium oxychloride ($ZrOCl_2$, AR, Tianjin Guangfu Fine Chemical Research Institute, Tianjin, China) was used as Zr precursor. Absolute ethanol (AR, Anhui Ante Biochemical Co., Ltd., Suzhou, Anhui, China), *N*′,*N*-dimethylformamide (DMF, AR, Tianjin Kermel Chemical Reagent Co., Ltd., Tianjin, China), and deionized water were used as solvents. Polyvinylpyrrolidone (PVP, M_w = 1 300 000) was purchased from Alfa Aesar (Ward Hill, MA, USA) and used as spinning agent.

Solution A was prepared by mixing PVP in 15 mL of absolute ethanol under stirring for 4 h. Solution B was prepared by mixing 2 g of $ZrOCl_2$ (2 g), 4 mL of DMF, and 1 mL of deionized water under stirring for 4 h. Solution B was gradually added to solution A, and the mixture was stirred for 2 h to obtain ZrO_2 precursor solutions with PVP contents of 3, 4, 5, and 6 wt%. The precursor solutions were then placed in the micropump of an electrostatic jet apparatus (KH-08, Beijing Kangsente Co. Ltd., Beijing, China) to obtain PVP/$ZrOCl_2$ composite nanofibers. A voltage of 18 kV was applied with a flow rate of 0.4 mL h^{-1}. The distance from the nozzle tip to the collector was 10 cm. The temperature of the electrospinning environment was 40 °C, and the humidity was maintained at 40%. The composite nanofibers were calcined at 500–700 °C for 2 h to form ZrO_2 nanofibrous membranes. The composite nanofibers were then calcined in vacuum to increase the surface isoelectric point.

Characterization

X-ray diffraction (XRD, Model 7000, Shimadzu Ltd., Japan) analysis with Cu K_α radiation (operating at 40 kV and 40 mA) was conducted to identify phases present in the ZrO_2 nanofibrous membranes. The morphologies of the resulting nanofibrous membranes were characterized by scanning electron microscopy (SEM, JSM 6700, Olympus, Tokyo, Japan). The pore size of the membranes and the diameter of the nanofibers were determined through surface measurement of the SEM images with SmileView (Software, JEOL, Japan). Fifty samples were tested to determine the pore size and diameter distribution. The ZrO_2 nanofibrous membranes were characterized with a model BK122T-B analyzer by N_2 adsorption analysis. The surface area of the membranes was evaluated with the Brunauer–Emmett–Teller (BET) model. JS94H-type micro electrophoresis apparatus was used to test the potential of ZrO_2 nanofibrous membranes and characterize their surface electrical properties. Electron binding energy of Zr 3d was also analyzed with X-ray photoelectron spectroscopy (XPS, AXIS-ULTRA DLD, Shimadzu Corporation, Tokyo, Japan) over the range of 0–1200 eV by using Al Kα radiation.

The adsorption and separation properties of the positively charged ZrO_2 nanofibrous membranes were characterized using titan yellow as the simulated virus. Titan yellow is a negatively charged pigment with two negative charges in its molecules;[20] this dye will be adsorbed on the surface of the positively charged material. Hence, interception rate and adsorption capacity for titan yellow can be used to evaluate the adsorption and separation properties of positively charged materials. Titan yellow solutions with different concentrations were prepared, and the absorbance standard curve was obtained using METASH UV-5100 UV visible spectrophotometer. Water flux was determined by Hydra MF/UF-type membrane flux meter. The volume of the membrane per unit area in unit time was obtained using eqn (1).

$$J = \frac{Q}{A\Delta t} \quad (1)$$

where, J is the water flux [L (m^2 h)$^{-1}$], Q is the volume of filtered water (L), A is the effective filtration area of membranes (m^2), and Δt is the test time (h). A 20 mL titan yellow solution (10 mg L^{-1}) was filtered using the positively charged ZrO_2 nanofibrous membranes under different pH conditions. The absorbance of the original solution and the filtered solution was determined, and interception rate was calculated using eqn (2).

$$R = \left(1 - \frac{A_1}{A_2}\right) \times 100\% \quad (2)$$

where R is the interception rate, A_1 is the absorbance of the original titan yellow solution, and A_2 is the absorbance of the filtered titan yellow solution. A 1 L titan yellow solution (10 mg L^{-1}) was filtered using the positively charged ZrO_2 nanofibrous membranes under different pH conditions to determine the adsorption capacity.

Results and discussion

Phase composition of ZrO_2 nanofibrous membranes

Fig. 1 shows the XRD patterns of ZrO_2 nanofibrous membranes before and after calcination. A broad diffraction peak appears at $2\theta = 25°$ before the calcination of the PVP/$ZrOCl_2$ composite nanofibers; this peak is the semi crystalline peak of PVP in the composite nanofibers. A dome-shaped diffraction peak was found at 2θ = 25–35° when the fibers were calcined at 500 °C. This finding indicates that the nanofibrous membranes remained amorphous. When calcined at 600 °C, the tetragonal phase of ZrO_2 was formed, and the obtained diffraction peaks of the nanofibrous membranes are consistent with those of JCPDS 17-0923. When calcined at 700 °C, the tetragonal crystal surface

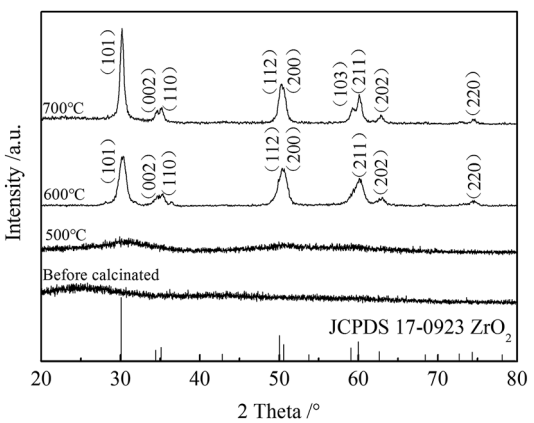

Fig. 1 XRD patterns of ZrO_2 nanofibrous membranes before and after calcinations.

(103) diffraction peak occurred at $2\theta = 59.28^{\circ}$, and the intensity of the crystalline peak of ZrO_2 increased.

Morphologies and physical properties of ZrO_2 nanofibrous membranes

Fig. 2 shows the morphologies of ZrO_2 nanofibrous membranes fabricated using precursor solutions with different PVP contents. A smooth nanofiber surface was obtained after calcination. The average diameter of the ZrO_2 nanofibers increases with increasing PVP content in the precursor solutions. This result is directly related to the diameter of the composite nanofibers fabricated by electrospinning.[21] Table 1 shows the viscosity, conductivity, and surface tension of the precursor solutions with different PVP contents and the average diameter of the composite nanofibers. The average diameter of the composite nanofibers increases with increasing PVP content. When the PVP content is 3 wt%, the viscosity of the precursor solution is only 245 mPa s. The viscous resistance of the precursor solution is low and insufficient to resist the stretching of the electric field force.[22] The jet splits in the tensile process, resulting in fine fibers with partial linear density distribution. The conductivity of the solution is 1947 μS cm^{-1}, which is beneficial to the stretching of the nanofiber; hence, the diameter of the composite nanofiber is small. With increasing PVP content, the viscosity of the precursor solution increases. The viscous resistance gradually increases, and the conductivity decreases, leading to increased nanofiber diameter. Fig. 3 shows the changes in the pore size formed after bonding of the nanofibers.

The pore size of the nanofibrous membranes affects the flux and is crucial to their adsorption and separation properties. With increasing PVP content, the pore size distribution of ZrO_2 fibers is uneven, and the average pore size decreases slightly. This finding could be due to increase in the diameter of ZrO_2 nanofibers (shown in insert images of Fig. 3) as the PVP content increases. Overlapped nanofibers are dense and decrease the pore size between nanofibers. Moreover, the distribution of ZrO_2 nanofibers fabricated by the precursor solution with high PVP content is uneven, and some nanofibers have large diameter, resulting in reduced pore size between nanofibers. The pore sizes of the ZrO_2 nanofibrous membranes are between 0.2 and 1.6 μm, which conform to the pore size range of the microfiltration membranes.

Table 1 Viscosity, conductivity, and surface tension of the precursor solutions with different PVP contents and average diameters of the fabricated composite nanofibers by electrospinning

PVP content (wt%)	3	4	5	6
Viscosity (mPa s)	245	335	507	628
Conductivity (μS cm^{-1})	1947	1750	1433	1396
Surface tension (mN m^{-1})	25.8	24.6	25.1	25.3
Average diameter (nm)	185.2	247.3	331.1	402.5

The specific surface area of ZrO_2 nanofibrous membranes affects their adsorption capacity and is related to the average diameter of ZrO_2 nanofibers. Fig. 4 shows the BET surface curves of ZrO_2 nanofibrous membranes with different average diameters of nanofibers. By determining the equilibrium adsorption capacity, the specific surface area of the sample was calculated using the theoretical model. The equilibrium adsorption capacity of nitrogen molecules on the sample surface was measured, and the monolayer saturated adsorption capacity was calculated by the BET theoretical model to determine the number of molecules. The equivalent maximum cross-sectional area of the nitrogen molecule was calculated using the

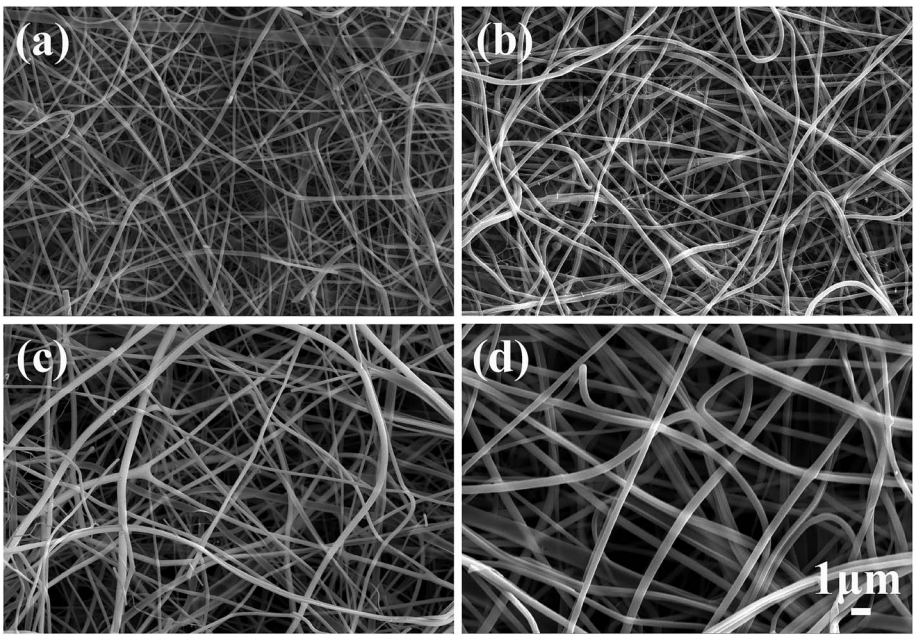

Fig. 2 Morphologies of ZrO_2 nanofibrous membranes obtained using precursor solutions with different PVP contents: (a) 3 wt%, (b) 4 wt%, (c) 5 wt%, and (d) 6 wt%.

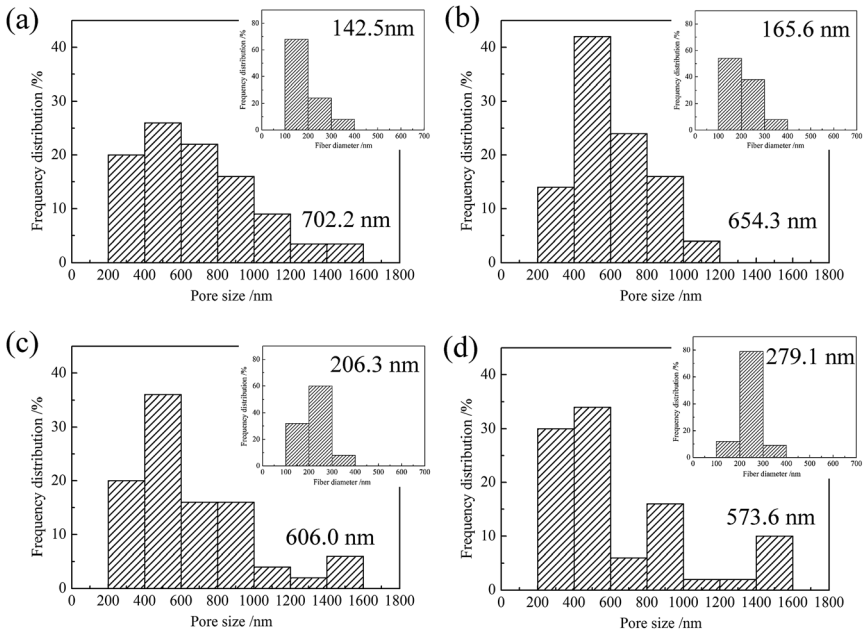

Fig. 3 Pore size distributions of ZrO_2 nanofibrous membranes obtained using precursor solutions with different PVP contents: (a) 3 wt%, (b) 4 wt%, (c) 5 wt%, and (d) 6 wt%. The inset images show the nanofiber diameter distributions.

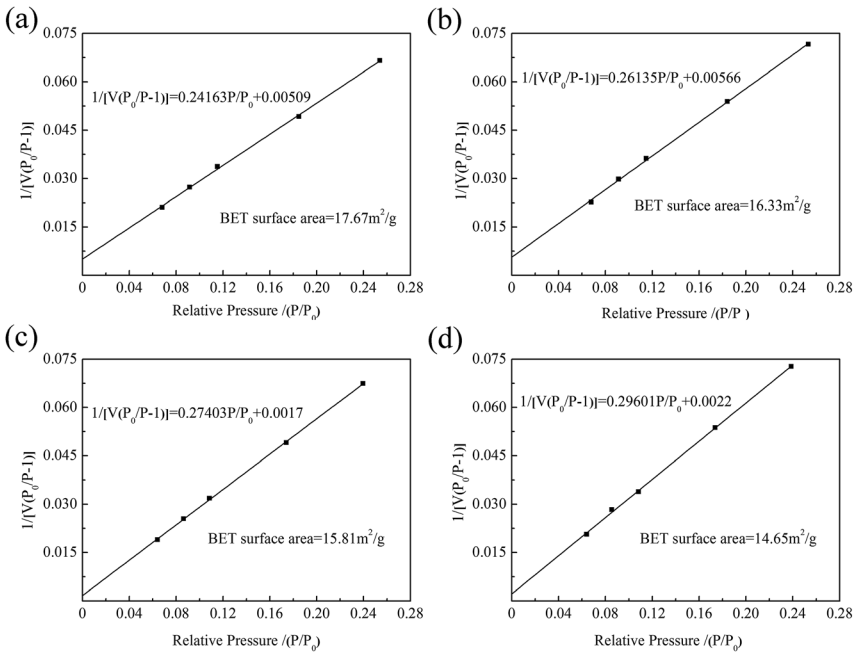

Fig. 4 BET surface curves of ZrO_2 nanofibrous membranes with different average diameters of nanofibers: (a) 142.5 nm, (b) 165.6 nm, (c) 206.3 nm, and (d) 279.1 nm.

surface-closed six-party model. The specific surface area of the sample was then obtained using eqn (3).

$$S_g = \frac{V_m N A_m}{22400 W} \times 10^{-18} \quad (3)$$

where S_g is the specific surface area, V_m is the single-layer saturated adsorption capacity of nitrogen molecules in standard conditions, N is the Fugadero constant (6.02×10^{23}), A_m is the equivalent maximum cross-sectional area of molecular nitrogen (theories value $A_m = 0.162$ nm), and W is the quality of the sample. The BET equation is as follows.

$$\frac{P}{V(P_0 - P)} = \frac{1}{V_m C} + \frac{C-1}{V_m C}\left(\frac{P}{P_0}\right) \quad (4)$$

where P is the nitrogen pressure, P_0 is the saturated vapor pressure of the sample, V is the actual adsorption amount of the sample, V_m is the single-layer saturated adsorption capacity of nitrogen molecules under standard conditions, and C is the parameter related to the adsorption capacity of the sample. The specific surface area of the ZrO_2 nanofibrous membranes decreases from 17.67 $m^2\ g^{-1}$ to 14.65 $m^2\ g^{-1}$ with increasing nanofiber diameter. When the average diameter of the ZrO_2 nanofibers is 142.5 nm, the maximum specific surface area of the membrane is 17.67 $m^2\ g^{-1}$. The specific surface area of the electrospun ZrO_2 nanofibrous membranes is higher by more than twice than that of conventional porous ceramic filter (8 $m^2\ g^{-1}$).[11] This finding is explained by the low porosity and surface area of traditional porous ceramic filters. The electrospun nanofibrous membranes exhibit the advantages of high specific surface area and porosity.

Positively charged properties of ZrO_2 nanofibrous membranes

The isoelectric point of metal oxide ceramics is used extensively in materials science in various aqueous processing steps. In the absence of chemisorbed or physisorbed species, particle surfaces in aqueous suspensions are generally assumed to be covered with surface hydroxyl species.[23] At pH values above the isoelectric point, the predominate surface species is $M–O^-$, whereas at pH values below the isoelectric point, $M–OH_2^+$ species predominate. Fig. 5 shows the zeta potential of ZrO_2 nanofibrous membranes at different pH values. The isoelectric point of ZrO_2 nanofibers obtained by atmospheric calcination is 4.3, whereas the isoelectric point is 4.8 when calcined in vacuum. Vacuum calcination can increase the isoelectric point of ZrO_2 nanofibrous membranes, which is related to the crystallization process of ZrO_2. The ratio of Zr atoms to O atoms is 1 : 1 in $ZrOCl_2$, and its decomposition process requires O_2 to participate. During vacuum calcination, oxygen vacancies existed in the resulting ZrO_2, which makes the isoelectric point move to the right. In the pH value solution below the isoelectric point, the surface of ZrO_2 nanofibers is covered with a positively charged group, and the zeta potential is positively charged. At low pH levels, the positive charge is high. When the pH value is 3, the zeta potential of the vacuum-calcined ZrO_2 nanofibrous membranes reaches 18.39 mV. The binding energy of Zr in ZrO_2 nanofibrous membranes calcined in different atmospheres was characterized (Fig. 6). The peaks of Zr 3d of vacuum-calcined ZrO_2 nanofibrous membranes shifted to the right compared with the atmospheric calcination; this finding indicates that the binding energy of Zr decreases. The decrease in binding energy generally indicates that the electron cloud density around the atom increases, and the valence state of oxide decreases.[24] This finding indirectly indicates that the number of oxygen vacancies in the vacuum-calcined ZrO_2 nanofibrous membranes is higher than that in the atmospheric calcined membranes. The more the oxygen vacancies, the higher zeta-positive potential of membranes and the higher the positive charge will be.

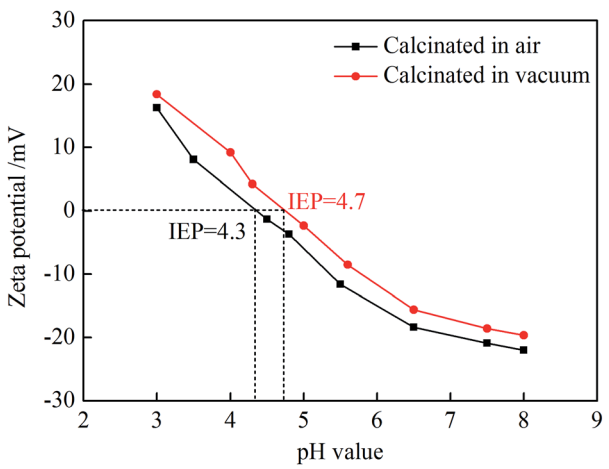

Fig. 5 Zeta potentials of ZrO_2 nanofibrous membranes at different pH values.

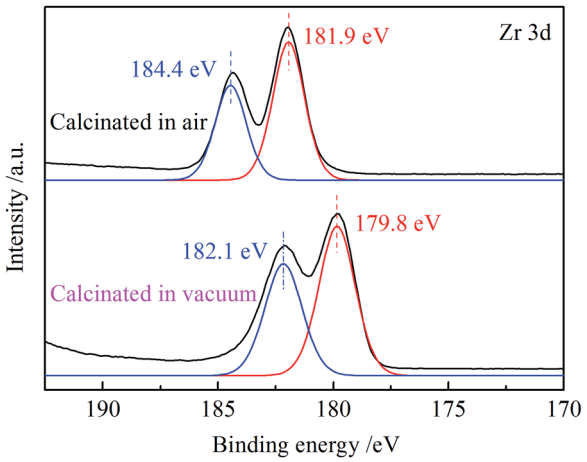

Fig. 6 XPS spectra of Zr 3d in ZrO_2 nanofibrous membranes obtained by calcination in different atmospheres.

Membrane flux of positively charged ZrO_2 nanofibrous membranes

Water flux can influence the filtration efficiency of nanofibrous membranes when used for adsorption separation. Large water flux requires short time to filter the same volume of solutions. Fig. 7 shows the water flux of ZrO_2 nanofibrous membranes with different average pore sizes. The effective filtration area of nanofibrous membranes is 12.56 cm^2, the membrane thickness is 1 mm, and the operation pressure is 1 Pa. The water fluxes increase with the increase of average pore size of ZrO_2 nanofibrous membranes, which were all above 500 L $(m^2\ h)^{-1}$. When the average pore size of ZrO_2 nanofibrous membranes is 702.2 nm, the maximum water flux can reach 523 L $(m^2\ h)^{-1}$. The water flux is five times higher than the traditional ceramic microporous filter membrane and the operation pressure is low.[25] The water flux of a filter membrane is mainly related to thickness, osmotic pressure, pore size, and porosity. Under the premise of certain membrane thickness and operating pressure, the larger the pore size, the smaller the permeate resistance and the easier the penetration of water molecules will be.

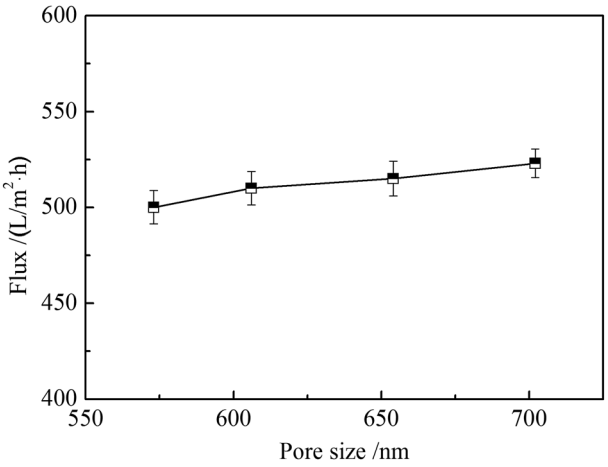

Fig. 7 Water flux of ZrO_2 nanofibrous membranes with different average pore sizes.

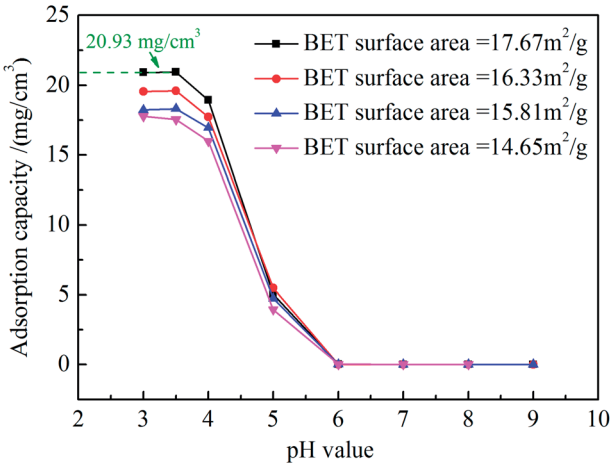

Fig. 9 Adsorption capacities of ZrO_2 nanofibrous membranes calcined in vacuum with different specific surface areas at different pH values.

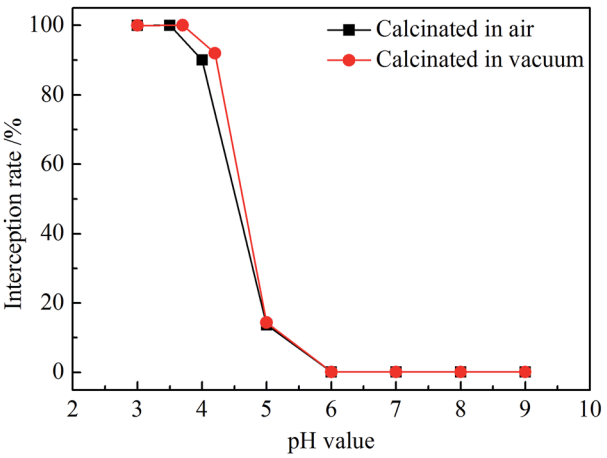

Fig. 8 Interception rates of ZrO_2 nanofibrous membranes at different pH values.

Therefore, the water flux is positively related to the pore size of nanofibrous membranes.

Adsorption and separation properties of positively charged ZrO_2 nanofibrous membranes

Fig. 8 shows interception rates of ZrO_2 nanofibrous membranes at different pH values. titan yellow interception rate of air-calcined ZrO_2 nanofibrous membranes remained above 99.99% in the solution with pH = 3.5, and the maximum interception rate was 99.996% in pH = 3 solution. The interception rate drops rapidly in the solution with pH > 4 and then tends to be smooth; the interception rate is only 0.08% in the solution with pH > 6. The interception rate of vacuum-calcined nanofibrous membranes for titan yellow is 99.997% in the solution with pH = 3–4. The interception rate of ZrO_2 nanofibrous membranes is closely related to the electrical properties of the nanofiber surface. The interception rate of vacuum-calcined nanofibrous membranes is similar to that calcined in the air, but the pH range for removing titan yellow is widened slightly due to the increase of the isoelectric point. The surface of ZrO_2 nanofibers carries positive charges in the solution of pH < IEP; titan yellow molecules with negative charge were adsorbed, and the interception rate is high. By contrast, the interception rate is low in pH > IEP solutions due to electrostatic repulsion.

Fig. 9 shows adsorption capacities of vacuum-calcined ZrO_2 nanofibrous membranes with different specific surface area at different pH values. The adsorption capacity of vacuum-calcined ZrO_2 nanofibrous membranes reached 20.93 mg cm^{-3} when its specific surface area was 17.67 m^2 g^{-1} in the solution with pH = 3–3.5. The saturated adsorption capacity decreased rapidly and is only about 0.01 mg cm^{-3} in the solution with pH > 6. The saturation adsorption capacity of ZrO_2 nanofibrous membranes for titan yellow is related to the isoelectric point and the specific surface area.[26] In generally, the specific surface area of nanofibrous membranes is mainly affected by the nanofiber diameter, and reducing the nanofiber diameter can improve its specific surface area. However, pore sizes formed by nanofibers bonding decrease when the diameter decrease excessively, which may affect the water flux of membranes. ZrO_2 nanofibrous membranes with high isoelectric point and high specific surface area have high adsorption capacity, which can prolong the service life of the filter.

Conclusions

Positively charged ZrO_2 nanofibrous membranes were fabricated by electrospinning; the highest specific surface area of the membranes is 17.67 m^2 g^{-1}. After vacuum calcination, the oxygen vacancies on the surface of nanofibers increased, and the isoelectric point of nanofibrous membranes increased from 4.3 to 4.7. The maximum water flux of the positively charged ZrO_2 nanofibrous membranes is 523 L (m^2 h)$^{-1}$ with an effective filtration area of 12.56 cm^2, a thickness of 1 mm, and an operating pressure of 1 Pa. The interception rate of vacuum-calcined

nanofibrous membranes for titan yellow is 99.997% in the solution with pH = 3–4, and its maximum saturated adsorption capacity reached 20.93 mg cm^{-3}. ZrO_2 nanofibrous membranes exhibit improved adsorption and separation performance compared with the traditional ceramic porous filter. These membranes have a wide application prospect in infectious virus protection, water treatment, pharmaceutical production, and biological engineering. However, in vacuum calcination, the spinning agent PVP cannot be completely decomposed and there may be residuals, which have an impact on the positively charge membrane. In addition, the isoelectric point of ZrO_2 nanofibrous membranes have to be improved further for treatment of neutral or alkaline sewage, which is the main research direction in the future.

Conflicts of interest

There are no conflicts to declare.

Acknowledgements

The authors would like to acknowledge the support from the National Natural Science Foundation of China (No. 51572217 and 51672211), the China Postdoctoral Science Foundation (No. 2015M582689) and the Postdoctoral Science Foundation of Shaanxi Province (No. 2016BSHEDZZ03).

References

1 B. Michen and T. Graule, Isoelectric points of viruses, *J. Appl. Microbiol.*, 2010, **209**, 388–397.
2 M. M. F. de Cortalezzi, M. V. Gallardo, F. Yrazu, G. J. Gentile, O. Opezzo, R. Pizarro, H. R. Poma and V. B. Rajal, Virus removal by iron oxide ceramic membranes, *J. Environ. Chem. Eng.*, 2014, **3**, 1831–1840.
3 A. Garrido, R. M. Pashley and B. W. Ninham, Low temperature MS2 (ATCC15597-B1) virus inactivation using a hot bubble column evaporator (HBCE), *Colloids Surf., B*, 2017, **151**, 1–10.
4 J. J. Borrego, R. Cornax, D. R. Preston, S. R. Farrah, B. Mcelhaney and G. Bitton, Development and application of new positively charged filters for recovery of bacteriophages from water, *Appl. Environ. Microbiol.*, 1991, **57**, 1218–1222.
5 J. Werner, B. Besser, C. Brandes, S. Kroll and K. Rezwan, Production of ceramic membranes with different pore sizes for virus retention, *Journal of Water Process Engineering*, 2014, **4**, 201–211.
6 A. Duek, E. Arkhangelsky, R. Krush, A. Brenner and V. Gitis, New and conventional pore size tests in virus-removing membranes, *Water Res.*, 2012, **46**, 2505–2514.
7 H. van der Laan, D. van Halem, P. W. M. H. Smeets, A. I. A. Soppe, J. Kroesbergen, G. Wubbels, J. Nederstigt, I. Gensburger and S. G. J. Heijman, Bacteria and virus removal effectiveness of ceramic pot filters with different silver applications in a long term experiment, *Water Res.*, 2014, **51**, 47–54.
8 N. Shirasaki, T. Matsushita, Y. Matsui, M. Kobuke and K. Ohno, Comparison of removal performance of two surrogates for pathogenic waterborne viruses, bacteriophage Qβ and MS2, in a coagulation–ceramic microfiltration system, *J. Membr. Sci.*, 2009, **326**, 564–571.
9 B. L. T. Lau, G. W. Harrington, M. A. Anderson and I. Tejedor, Removal of nano and microparticles by granular filter media coated with nanoporous aluminium oxide, *Water Sci. Technol.*, 2004, **20**, 223–228.
10 M. Wegmann, B. Michen, T. Luxbacher, J. Fritsch and T. Graule, Modification of ceramic microfilters with colloidal zirconia to promote the adsorption of viruses from water, *Water Res.*, 2008, **429**, 1726–1734.
11 M. Wegmann, B. Michen and T. Graule, Nanostructured surface modification of microporous ceramics for efficient virus filtration, *J. Eur. Ceram. Soc.*, 2008, **28**, 1603–1612.
12 H. Ma, B. S. Hsiao and B. Chu, Functionalized electrospun nanofibrous microfiltration membranes for removal of bacteria and viruses, *J. Membr. Sci.*, 2014, **452**, 446–452.
13 W. Huang, Y. Wang, C. Chen, J. L. M. Law, M. Houghton and L. Chen, Fabrication of flexible self-standing all-cellulose nanofibrous composite membranes for virus removal, *Carbohydr. Polym.*, 2016, **143**, 9–17.
14 K. Yoo, K. Kim, X. Wang, D. Fang and B. S. Hsiao, High flux ultrafiltration membranes based on electrospun nanofibrous PAN scaffolds and chitosan coating, *Polymer*, 2006, **47**, 2434–2441.
15 R. Gopal, S. Kaur, Z. Ma, C. Chan, S. Ramakrishna and T. Matsuura, Electrospun nanofibrous filtration membrane, *J. Membr. Sci.*, 2006, **281**, 581–586.
16 C. Gong, H. Liu, B. Zhang, G. Wang, F. Cheng, G. Zheng, S. Wen, Z. Xue and X. Xie, High level of solid superacid coated poly(vinylidene fluoride) electrospun nanofiber composite polymer electrolyte membranes, *J. Membr. Sci.*, 2017, **535**, 113–121.
17 Z. Ma, M. Kotaki and S. Ramakrishna, Electrospun cellulose nanofiber as affinity membrane, *J. Membr. Sci.*, 2005, **265**, 115–123.
18 M. Guo, B. Ding, X. Li, X. Wang and J. Yu, Amphiphobic nanofibrous silica mats with flexible and high-heat-resistant properties, *J. Phys. Chem. C*, 2010, **114**, 916–921.
19 M. S. Islam, J. R. McCutcheon and M. S. Rahaman, A high flux polyvinyl acetate-coated electrospun nylon 6/SiO_2 composite microfiltration membrane for the separation of oil-in-water emulsion with improved antifouling performance, *J. Membr. Sci.*, 2017, **537**, 297–309.
20 X. Cheng, N. Li, M. Zhu, L. Zhang, Y. Deng and C. Deng, Positively charged microporous ceramic membrane for the removal of titan yellow through electrostatic adsorption, *J. Environ. Sci.*, 2016, **44**, 204–212.
21 S. V. Fridrikh, J. H. Yu, M. P. Brenner and G. C. Rutledge, Controlling the fiber diameter during electrospinning, *Phys. Rev. Lett.*, 2003, **90**, 144502.

22 A. F. Spivak, Y. A. Dzenis and D. H. Reneker, A model of steady state jet in the electrospinning process, *Mech. Res. Commun.*, 2000, **27**, 37–42.

23 D. A. H. Hanaor, M. Michelazzi, C. Leonelli and C. C. Sorrell, The effects of carboxylic acids on the aqueous dispersion and electrophoretic deposition of ZrO_2, *J. Eur. Ceram. Soc.*, 2012, **32**, 235–244.

24 K. Zhao, L. Teng, Y. Tang and X. Chen, Branched titanium oxide/vanadium oxide composite nanofibers formed by electrospinning and dipping in vanadium sol, *Ceram. Int.*, 2014, **140**, 5335–15340.

25 H. Chang, H. Liang, F. Qu, B. Liu, H. Yu, X. Du, G. Li and S. A. Snyder, Hydraulic backwashing for low-pressure membranes in drinking water treatment: a review, *J. Membr. Sci.*, 2017, **540**, 362–380.

26 J. Kim, D. Kim, W. Lee, Y. Lee and H. Kim, Impact of total organic carbon and specific surface area on the adsorption capacity in Horn River shale, *J. Pet. Sci. Eng.*, 2017, **149**, 331–339.